Quasi-Fermi level pinning in interband cascade lasers

Yuzhe Lin, Lu Li, Wenxiang Huang, *Student Member, IEEE*, Rui Q. Yang, *Fellow*, *IEEE*, James A. Gupta, Wanhua Zheng, *Member, IEEE*

***Abstract*—A systematic study of the quasi-Fermi level pinning in various interband cascade lasers (ICLs) is reported. These ICLs, with either type-II or type-I quantum well active regions, cover the mid-infrared wavelength range from 3 to 6 μm and can operate in continuous wave (cw) at room temperatures and above. It was found that the quasi-Fermi level can be pinned in many ICLs over a wide range of temperature, which is associated with an observed drop of differential resistance at threshold. For the first time, the quasi-Fermi level pinning was demonstrated in ICLs at room temperature. The temperature dependence of the quasi-Fermi level pinning in ICLs was also examined. A pinning factor is introduced to evaluate how well the quasi-Fermi level is pinned in ICLs with different configurations and lasing wavelengths. Also, it was found that the quasi-Fermi level pinning disappeared in some ICLs where an obvious drop of differential resistance could not be observed at the threshold. Furthermore, the quasi-Fermi level pinning was found to be correlated to the doping concentration in electron injectors in ICLs. Possible mechanisms and implications related to the quasi-Fermi level pinning are discussed.**

***Index Terms*—Interband cascade laser, quasi-Fermi level pinning, semiconductor heterostructure, quantum well.**

I. Introduction

In recent years, even with the relative immaturity of the Sb-based material system, interband cascade lasers (ICLs) [1] have been developed with excellent device performance in the mid-infrared (IR) wavelength range from 3 to 6 μm [2-3]. By combining the advantages of quantum cascade lasers (QCLs) and interband diode lasers, ICLs achieved cw operation at temperatures up to 115°C with low threshold-current densities (*e.g.* 100 A/cm^2 at 300 K), low power consumption (<0.1 W at threshold at 300 K), and cw output power exceeding 500 mW [2]. Single-mode distributed feedback (DFB) ICLs [4-6] have been developed and used in various situations for measuring important gases such as H_2CO, C_2H_6, CH_4 and HCl [7-11]. ICLs are becoming the choice of mid-IR laser source for many practical applications such as chemical sensing, imaging and industrial processing control. However, the ICL is still a relatively new type of semiconductor laser, even though it was initially proposed in 1994 [1] – more than 20 years ago. This is partially due to the less mature Sb-based III-V materials and related device fabrication technology for ICLs, as well as limited resources for the growth of Sb-based materials compared to mature InP- and GaAs-based material systems. Although ICLs have some similarities with both QCLs and conventional diode lasers there are also very significant differences. For example, with the type-II broken-gap hetero-structure for interband tunneling between cascade stages [12], carrier transport and generation in ICLs are quite different from the mechanisms in QCLs and conventional diode lasers. Consequently, many aspects of ICLs have been unexplored or remain in the early phase. One of those aspects is the quasi-Fermi level (carrier concentration) pinning (due to optical gain pinning) at threshold, which is fundamentally related to carrier dynamics. How well quasi-Fermi level is pinned at threshold has important consequences on the laser device performance. However, there was not any focused study of quasi-Fermi level pinning in ICLs, except one paper [13] in which a lack of pinning of the spontaneous emission was reported for an ICL at temperatures above 180 K, implying a continued increase of the carrier concentration (N) above the threshold. The increase of N with injection current beyond the threshold would increase the internal loss, which might be a main mechanism responsible for the observed efficiency droop in ICLs at high current densities [14]. Also, a lack of the quasi-Fermi level pinning could imply extra carrier loss and incomplete carrier injection [15]. Hence, it is meaningful to investigate the quasi-Fermi level pinning in ICLs and its dependence on temperature, which may help to gain understanding and insights into details of the underlying physics and to advance the development of ICL technology for more applications.

In this paper, we report a systematic examination of the quasi-Fermi level pinning in various ICLs with different design configurations in a wide lasing wavelength range from 3 to 6 μm. These ICLs have either type-II quantum well (QW) or type-I QW active regions, which were grown on GaSb or InAs substrates. Based on extracted electrical derivative characteristics, we can obtain features related to the quasi-Fermi level pinning in ICLs over a wide range of temperature. The details of these features and relevant discussion are beneficial for further study and development of ICLs.

Manuscript received March 30, 2020; This work was supported in part by the National Science Foundation (NSF) under Grant ECCS-1931193.

Y. Lin is with Institute of Semiconductors, Chinese Academy of Sciences and the College of Materials Science and Opto-Electronic Technology, University of Chinese Academy of Sciences, Beijing, China, and the School of Electrical and Computer Engineering, University of Oklahoma.

L. Li was with the School of Electrical and Computer Engineering, University of Oklahoma. He is now with Lumentum, Milpitas, CA.

W. Huang is with both the School of Electrical and Computer Engineering and Department of Physics and Astronomy, University of Oklahoma, Norman.

R. Q. Yang is with the School of Electrical and Computer Engineering, University of Oklahoma, Norman, OK (Rui.q.Yang@ou.edu).

J. A. Gupta is with the National Research Council of Canada, Ottawa, ON.

W. Zheng is with Institute of Semiconductors, Chinese Academy of Sciences, Beijing, China.

II. Theoretical Framework and Measurement Model

As discussed in Ref. [16], the current (I) - voltage (V) characteristics in a cascade stage can be described by

$$I = I_0(e^{qV/kT} - 1) \quad (1)$$

where q is the electron charge, k is the Boltzmann constant, T is temperature, and I_0 is the saturation current, which is determined by the carrier concentration and the carrier lifetime due to various scattering mechanisms. For an ICL with N_c identical cascade stages, which is connected in series from the equivalent circuit perspective [17], an external bias voltage V is equally shared by all stages and then Eq. (1) can be written as

$$I = I_0(e^{qV/N_c kT} - 1) \quad (2)$$

Qualitatively, this is similar to the diode equation for a *p-n* junction in an ideal case. Considering possible deviations from the ideal case, an ideality factor n could be introduced so that Eq. (2) is rewritten as

$$I = I_0(e^{qV/nN_c kT} - 1) \quad (3)$$

Usually, n is between 1 and 2, and will approach 2 when Shockley-Read-Hall (SRH) recombination is dominant with a high defect density in the material. Eq. (3) will be used to evaluate I-V characteristics of ICLs coupled with a series resistance R. Similar to the diode laser [18], the differential resistance of an ICL before the threshold can be expressed as

$$\frac{dV}{dI} = R + \frac{nN_c kT}{q}\frac{1}{I+I_0} \quad (4)$$

At threshold, the optical gain is pinned and thus the carrier concentration should be fixed according to the laser theory, and the quasi-Fermi level is pinned for every cascade stage. Consequently, the second term in Eq. (4) is diminished and then above the threshold, the differential resistance is

$$\frac{dV}{dI} = R \quad (5)$$

Hence, at threshold the differential resistance has an abrupt drop ΔR_{th}, given by

$$\Delta R_{th} = \frac{nN_c kT}{q}\frac{1}{I_{th}+I_0} \approx \frac{nN_c kT}{q}\frac{1}{I_{th}} \quad (6)$$

as I_0 is usually much smaller than the threshold current I_{th}. Thus, the drop ΔR_{th} can be used to evaluate how well the quasi-Fermi level is pinned and is inversely proportional to I_{th}. In a single-stage mid-IR laser, I_{th} is usually higher than 300 mA at 300 K, resulting in a value of ΔR_{th} less than 0.09 Ω with n=1. To have a standard without relying on a specific threshold current, it is more convenient to plot $I\mathrm{d}V/\mathrm{d}I$ as a function of current I. Noticing that $I_0 << I_{th}$, when I approaches I_{th} one can have

$$I\frac{dV}{dI} \approx IR + \frac{nN_c kT}{q} \quad (7)$$

So, at threshold, $I\mathrm{d}V/\mathrm{d}I$ will have a drop $I_{th}\Delta(\mathrm{d}V/\mathrm{d}I)_{th}$ that is proportional to the number of cascade stages and temperature without relying on the current and lasing wavelength. To give a fair assessment of the quasi-Fermi level pinning for devices with different numbers of cascade stages, a pinning factor

$$P_f = \Delta\left(I\frac{dV}{dI}\right)_{th} q/N_c\, kT \quad (8)$$

is introduced, which is equal to the ideality factor n if the quasi-Fermi level is completely pinned at threshold. So, in an ideal case, P_f is between 1 and 2 for a complete pinning. In a real device, P_f could be much higher than 2 with a high leakage current from side walls, which adds to the threshold current. Since the leakage current does not go through the bulk of the active region, it needs to be minimized for extracting the intrinsic value of P_f, which can be effectively done with broad-area devices as shown in section III.

In the next section, detailed results of electrical derivative characteristics extracted from *I-V* curves for various ICLs will be presented. These measurements were performed in LN_2 cryostats where heat-sink temperature can be controlled and adjusted over a wide temperature range from 80 to 400 K. The abrupt drop of differential resistance has not been observed and reported for mid-IR diode lasers at room temperature. This might be due to very small differential resistance in a mid-IR laser at high temperatures in contrast to that in a near IR laser and a lack of high-performance room temperature mid-IR diode lasers. ICLs with many stages alleviate the issue of very small differential resistance. But still, measurements need to be carried out carefully with stable and precision instruments. The experiments used an ILX Lightwave LDP-3811 precision current source and Keithley 2100 voltmeter. In order to minimize the influence of small temperature variations during cw operation, the sample temperature was allowed to stabilize before the measurement of each *I-V* curve.

III. Experimental Results and Discussion

The various ICLs that were examined are summarized in Table I with relevant design and characterization parameters. These ICLs were made over more than 15 years with different device configurations, some of which were reported previously for their exemplary device performance. The variety of these different ICLs enables the development of a broad overview of the phenomenon of quasi-Fermi level pinning.

TABLE I
Parameters of Wafers and Performance Features of Broad-area and Narrow Ridge Devices

Wafer	Type	Nc	λ[a] (μm)	J_{th}[b] (A/cm²)	substrate	Ref.
J732	Type-II	12	3.34	630	GaSb	[19]
R048	Type-II	10	5.3	2700	InAs	[27]
R049	Type-II	10	5.3	2350	InAs	[27]
V1046	Type-I	6	3.19	310	GaSb	[28]
V1081	Type-I	6	3.16	236	GaSb	*
V1082	Type-I	6	3.16	243	GaSb	*
V1191	Type-II	10	4.58	290	InAs	[3]
V1192	Type-II	15	6.0	333	InAs	[3]
V1215	Type-II	15	6.26	395	InAs	[3]
Adv01	Type-II	7	3.38	143	GaSb	[*,30]

[a]Pulsed lasing wavelength at 300 K except R049 at 295 K.
[b]Pulsed threshold current density at 300K except R049 at 295K.
*Internal testing report at the University of Oklahoma

A. Early Type-II ICLs on a GaSb substrate

Early ICLs were mostly based on a simple three-layer waveguide structure [12] with a relatively low n-type doping level (*e.g.* 1.5-3.0 $\times 10^{17}$ cm^{-3}) in the electron injection region. Here, we focus on devices made from wafer J732, which lased

in pulsed mode at temperatures up to 350 K [19]. This ICL wafer has 12 cascade stages, each of which comprises an AlSb/InAs/GaInSb/InAs/AlSb W-QW [20-21] active region for lasing emission near 3.3 μm at room temperature. The waveguide region is sandwiched between two InAs/AlSb superlattice (SL) cladding layers. In cw operation, narrow-ridge (NR) and broad-area (BA) devices lased at temperatures up to 237 and 172 K, respectively. More details of the device performance features were described in Ref. 19. The electrical derivative characteristics were extracted from the measured cw I-V curves. The extracted differential resistance and $I\mathrm{d}V/\mathrm{d}I$ for two representative BA and NR devices at various temperatures are shown in Fig. 1 and Fig. 2, respectively. As is clearly illustrated, the differential resistance and $I\mathrm{d}V/\mathrm{d}I$ exhibit sharp drops at threshold in these ICLs at all cw operating temperatures. The drop became somewhat less pronounced at a temperature close to the maximum cw operating temperature, which was more notable for BA devices in which thermal dissipation is less efficient.

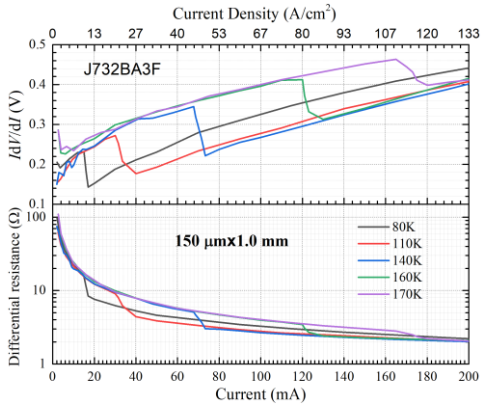

Fig. 1. Differential resistance (bottom) and $I\mathrm{d}V/\mathrm{d}I$ (top) for a BA device from J732 in cw operation at various heat-sink temperatures.

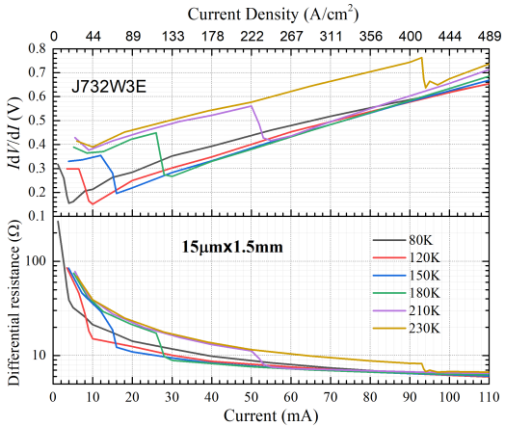

Fig. 2. Differential resistance (bottom) and $I\mathrm{d}V/\mathrm{d}I$ (top) for a NR device from J732 in cw operation at various heat-sink temperatures.

The differential resistance drop ΔR_{th} as a function of temperature is plotted in Fig. 3 for several devices with different sizes. Also included in Fig. 3 is the product of ΔR_{th} and the device area A, which is more meaningful in terms of its intrinsic property and less sensitive to device size. The value of ΔR_{th} had some uncertainties or relatively large inaccuracies for narrow ridge devices at low temperatures (e.g. 80 K) because their threshold currents were very low (a few mA) so that the instruments (current source and voltage meter) in the experiment did not have sufficient stability and accuracy to precisely determine a derivative at the threshold. Most extracted values of $\Delta R_{\mathrm{th}}A$ from BA devices are consistent, while it has some relatively large variations for NR devices at low temperatures (≤100 K) due to low threshold currents and possible leakage current via etched side walls associated with imperfect passivation. This is also reflected in the extracted pinning factor plotted in Fig. 4.

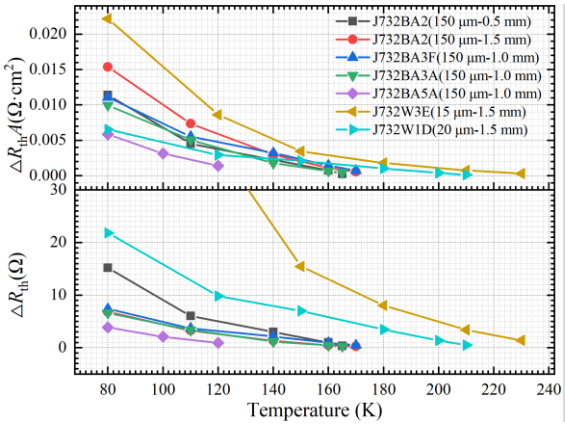

Fig. 3. ΔR_{th} and $\Delta R_{\mathrm{th}}A$ as a function of temperature for devices from J732.

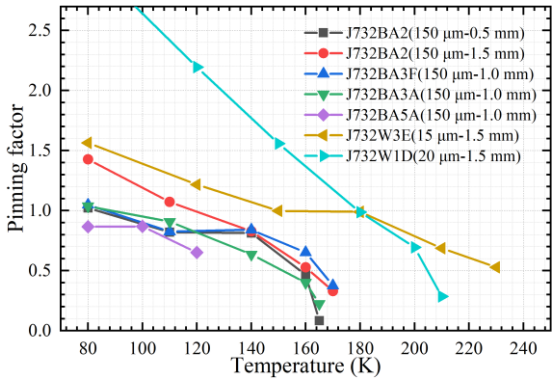

Fig. 4. Pinning factor as a function of temperature for devices from J732, where a NR device J732W1D had a relatively high threshold current density of 42A/cm², indicating a high percentage of leakage current and resulting in a high value of $I_{\mathrm{th}}\Delta R_{\mathrm{th}}$.

As shown in Fig. 4, the extracted value of P_f was abnormally high for a NR device J732W1D at low temperatures (*e.g.* P_f>3 at 80 K). This is because of a significantly higher threshold current density (42A/cm² at 80K) compared to that (~10 A/cm²) in BA devices, indicating a high percentage of leakage current (from side walls) that added to I_{th} and caused a high value of $I_{\mathrm{th}}\Delta R_{\mathrm{th}}$. If the leakage current could be deducted, the pinning factor would be lowered to a reasonable value. In a BA device or at high temperature, the bulk resistance became smaller and the side wall leakage current effect was reduced. Hence, putting data together from both BA and NR devices, we can deduce that the quasi-Fermi level was pinned at threshold in these ICLs over a wide temperature range of cw operation. The degree of pinning was reduced when the heat-sink temperature was close to the maximum cw operating temperature. This could be due to substantial heat accumulation inside an ICL, which raised the actual device temperature [22] and may not be the same in different stages. Consequently, the differential resistances of

individual stages might be changed at different currents so that the pinning happened modestly over an expanded current range near the threshold, which made it difficult for the instrument to detect. Alternatively, the quasi-Fermi level could be unpinned or incompletely pinned at a high injection current density due to carrier heating as discussed by Vinnichenko *et al*. regarding observed lack of the carrier density pining in conventional non-cascade type-I QW mid-infrared lasers [23].

It is worth noting that the abrupt drops in the differential resistances at threshold were initially observed in earlier ICLs operating at low temperatures [24-25] although the Fermi level pinning was not discussed there. Later, two sequential drops of the differential resistance at two threshold currents were observed from a dual-wavelength ICL with GaSb separate confinement layers (SCLs) [26].

B. Early Type-II ICLs on InAs substrates

ICLs made from wafers R048 and R049 (wafers B and A in [27]) had a low n-type doping (1.5×10^{17}cm^{-3}) in the electron injection regions and lased in pulsed mode at room temperature near 5.3 μm [27]. Both ICL wafers have 10 cascade stages sandwiched between two undoped InAs SCLs with highly doped n^{+}-InAs layers as cladding/contact layers. The wafers differ primarily in their top waveguide cladding designs. Ridge waveguide (width between 15 to 40 μm) devices from the two wafers lased in cw at temperatures up to 247 K. More details of the device performance and ICL structures were described in Ref. 27. Their electrical derivative characteristics were extracted from the measured cw I-V curves. The extracted differential resistance and IdV/dI for two representative devices (one from each wafer) at various temperatures are plotted in Fig. 5 and Fig. 6, where abrupt drops in differential resistance and IdV/dI can be seen at threshold in these ICLs at their cw operating temperatures. Similar to what observed in devices from J732, the drop became less pronounced at a temperature close to the maximum cw operating temperature.

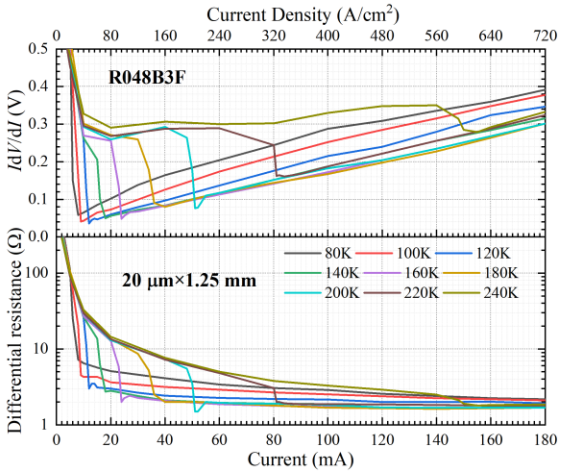

Fig. 5. Differential resistance (bottom) and IdV/dI (top) for a NR device from R048 in cw operation at various heat-sink temperatures.

Compared to J732, although the lasing wavelength is longer with the narrower bandgap, the differential resistance drop ΔR_{th} and the corresponding $\Delta R_{th}A$ are comparable to what observed in devices from J732, which are shown as a function of temperature in Fig. 7. This is because wafers R048 and R049 have relatively high surface defect densities (>2×10^{5}/cm^{2}) with an ideality factor exceeding unity. For this reason and to reduce the number of defects in ICLs, BA devices were not made from the two wafers. To reduce possible uncertainties of extracted derivatives for devices with a low threshold current at low temperatures, device R048B3F in Fig. 5 was recently measured again with more sampling points near the threshold. Its threshold currents at various temperature did not change, but the extracted differential resistance (red points) is more accurate, which is in good agreement with the earlier data (black points) for the device at temperatures higher than 120K as shown in Fig. 7. Also included in Fig. 7 is another NR device from R049. The extracted pinning factors in these ICLs at different temperatures are plotted in Fig. 8. P_f is higher than 2.5 for two ICLs from R049 at 80 K, which might be caused by some leakage current from side walls and limited accuracy with very small currents. At temperatures above 100 K, these ICLs had quite consistent value of P_f near 1.5, which is higher than that in J732 due to a higher ideality factor in R048 and R049 with high defect densities. P_f decreased with temperature T, especially when T was close to the maximum cw operating temperature. Hence, the quasi-Fermi level pining in these relatively long wavelength InAs-based ICLs is similar to devices made from J732.

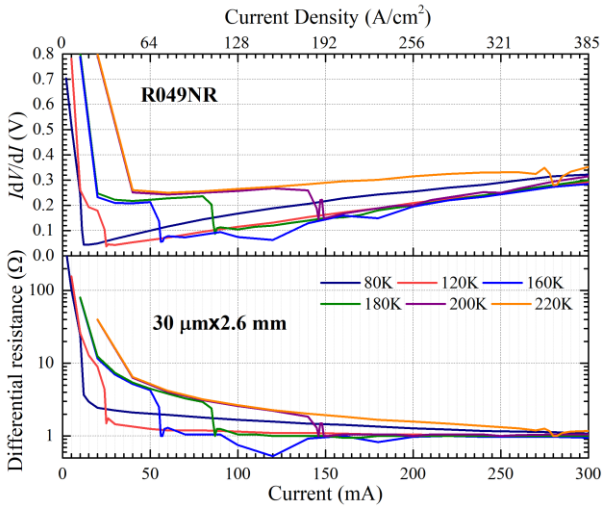

Fig. 6. Differential resistance (bottom) and IdV/dI (top) for a NR device from R049 in cw operation at various heat-sink temperatures.

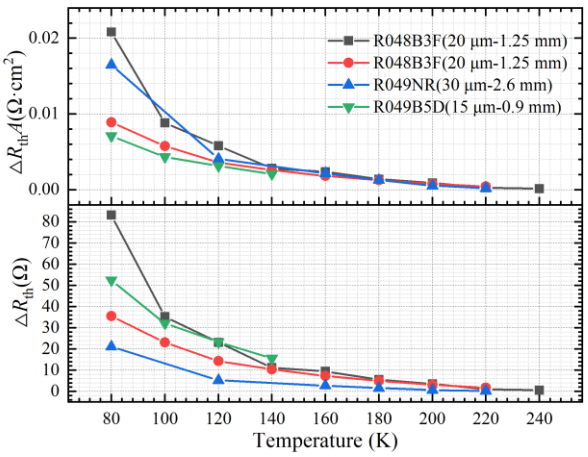

Fig. 7. ΔR_{th} and $\Delta R_{th}A$ as a function of temperature for devices from R048 and R049. Red and green points are recently measured data.

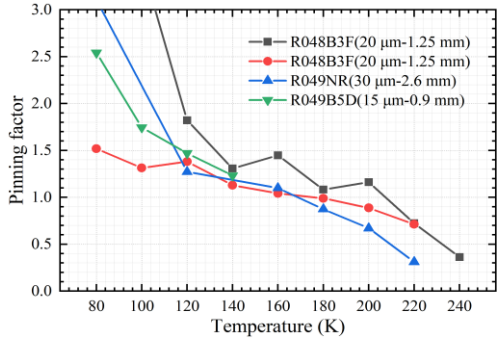

Fig. 8 Pinning factor as a function of temperature for devices from R048 and R049. Red and green points are recently measured data.

C. *Type-I ICLs on GaSb substrates*

This section reports a study of ICLs made from three wafers, V1046, V1081 and V1082. They had 6 cascade stages grown on GaSb substrates with the essentially same active regions based on AlAsSb/$Ga_{0.45}In_{0.55}As_{0.22}Sb_{0.78}$ type-I QWs with lasing wavelength near 3.2 μm at 300 K. ICLs made from V1046 were reported previously in Ref. 28. BA devices made from them had low threshold current densities at 300 K as shown in Table I. NR devices could lase in cw at 300 K and above. Their electrical derivative characteristics were extracted from the measured cw *I*-*V* curves. The extracted differential resistance, IdV/dI, and output power for three representative devices at various temperatures are plotted in Figs. 9-11. Abrupt drops in differential resistance and IdV/dI were observed at threshold in these type-I ICLs at all operating temperatures up to 300 K in cw mode. It is the first time that a clear drop of differential resistance at threshold was observed in ICLs at such a high temperature. Again, these drops became somewhat less pronounced at a temperature close to the maximum cw operating temperature. The values of ΔR_{th} and the corresponding $\Delta R_{th}A$ are comparable to what observed in devices from J732, which are shown as a function of temperature in Fig. 12. Compared with that in devices made wafer J732, threshold current densities in these type-I ICLs were significantly lower and consequently according to Eqs. (7) and (8) the pinning factor P_f in type-I ICLs is somewhat lower as shown in Fig. 13. Although there were variations with different sizes, multiple devices provided values of P_f consistently less than 0.8. From the measured output powers of these ICLs at relative low temperatures, which increased linearly with the injection current as shown in Figs. 9-11, their slope efficiencies were nearly unchanged with current. This suggested that the carrier concentration (and the quasi-Fermi level) was pinned in these ICLs at threshold over a wide range of operating temperature. The reason that P_f is less than unity in these ICLs might be associated with a high *n*-type doping concentration (2.3×10^{18} cm^{-3}) in the electron injectors based on the carrier rebalancing approach [29]. Such a high doping changed the carrier distribution so that the carrier transport deviated somewhat from the simple relationship between current and voltage based on Eq. (3). However, Eq. (3) can still be used to approximately describe carrier transport with a reduced ideality factor *n* compared to ICLs with a low *n*-type doping. It is also possible that the quasi-Fermi energy had substantial variations over an individual cascade stage under a forward bias and consequently only part of the quasi-Fermi level for a particular local electron density was pinned at threshold. Another possibility is incomplete carrier injection [15] with the high doping. Further investigation of carrier transport with different doping levels in the electron injectors is required to understand this.

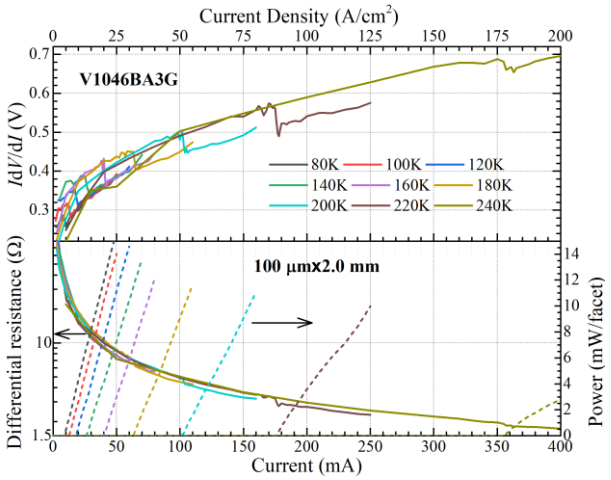

Fig. 9. Differential resistance (bottom), output power (bottom right axis) and IdV/dI (top) for a BA device from V1046 in cw operation at various heat-sink temperatures.

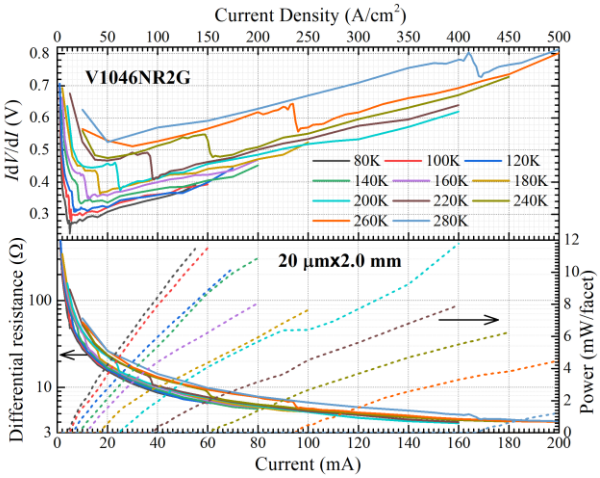

Fig. 10. Differential resistance (bottom), output power (bottom right axis) and IdV/dI (top) for a NR device from V1046 in cw operation at various heat-sink temperatures

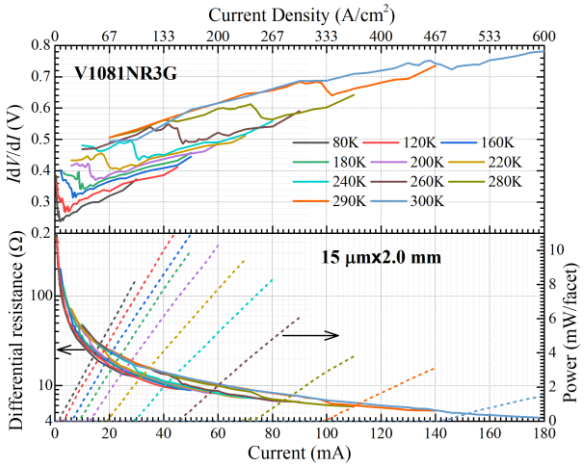

Fig. 11. Differential resistance (bottom), output power (bottom right axis) and IdV/dI (top) for a NR device from V1081 in cw operation at various heat-sink temperatures

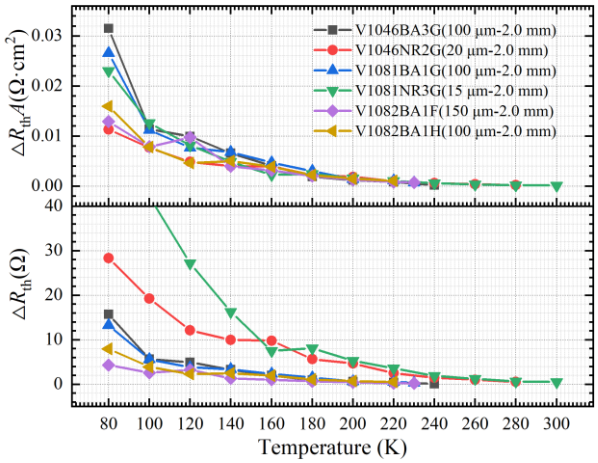

Fig. 12. ΔR_{th} and $\Delta R_{th}A$ as a function of temperature for devices from type-I ICL wafers.

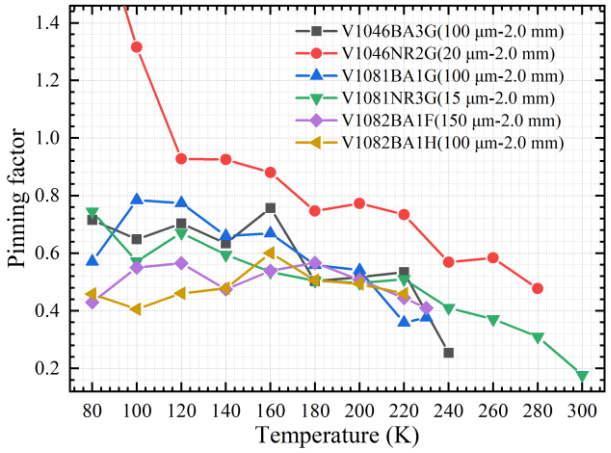

Fig. 13. Pinning factor as a function of temperature for devices from type-I ICL wafers, where high values of P_f for a NR device at 80 and 100 K were caused by limited precision with very small current.

D. Recent Type-II ICLs on InAs substrates

These recent InAs-based ICLs have an advanced waveguide configuration with relatively high n-type doping (2.6×10^{18} to 3.9×10^{18} cm^{-3}) in electron injection regions [3]. ICLs made from wafers V1191, V1192 and V1215 comprise 10 and 15 stages, respectively as indicated in Table I and were grown on InAs substrates with excellent material quality as reported [3]. BA devices were made from the three wafers and could lase over a wide temperature range from 80 K to above room temperature in pulsed mode. Their lasing wavelengths covers from 3.95 (80 K) to 4.85 μm (369 K) for V1191, 5.0 (80 K) to 6.27 μm (357 K) for V1192, and 5.2 (80 K) to 6.44 μm (335 K) for V1215. They exhibited low threshold current densities at 300 K as shown in Table I. NR devices were made only from two wafers V1191 and V1192 and could lase in cw at room temperature. More details can be found in Ref. 3. Their electrical derivative characteristics were extracted from the measured cw *I-V* curves. The extracted differential resistance, *IdV*/d*I* and output power for four representative devices at various temperatures are plotted in Figs. 14-17.

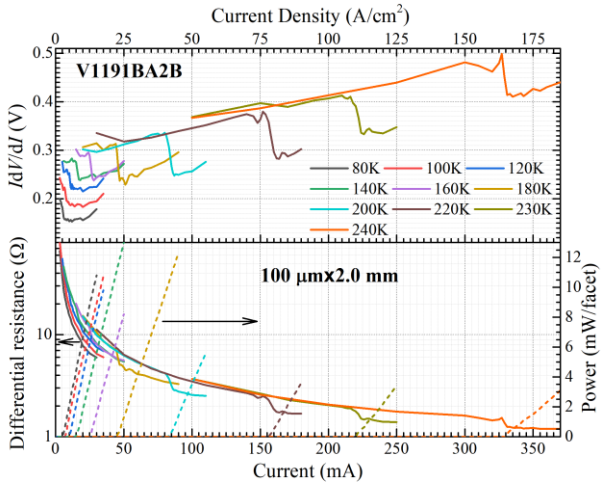

Fig. 14. Differential resistance (bottom), output power (bottom right axis) and *IdV*/d*I* (top) for a BA device from V1191 in cw operation at various heat-sink temperatures.

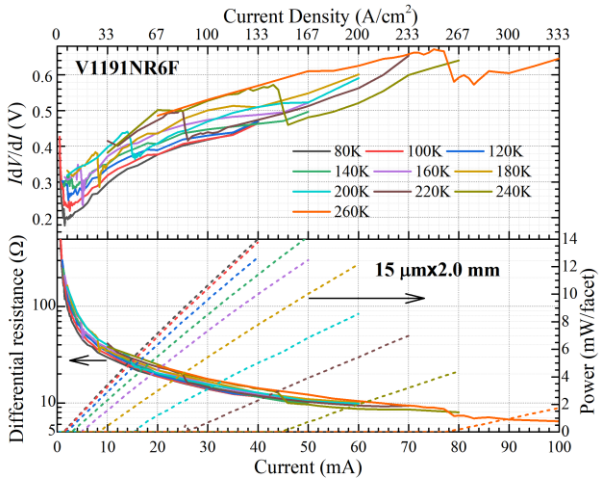

Fig. 15. Differential resistance (bottom), output power (bottom right axis) and *IdV*/d*I* (top) for a NR device from V1191 in cw operation at various heat-sink temperatures.

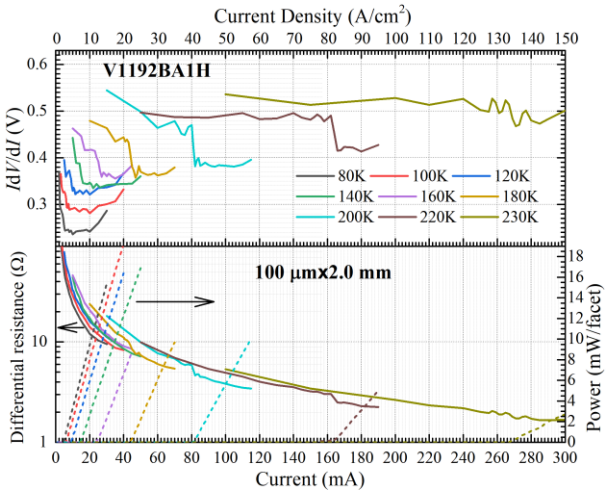

Fig. 16. Differential resistance (bottom), output power (bottom right axis) and *IdV*/d*I* (top) for a BA device from V1192 in cw operation at various heat-sink temperatures.

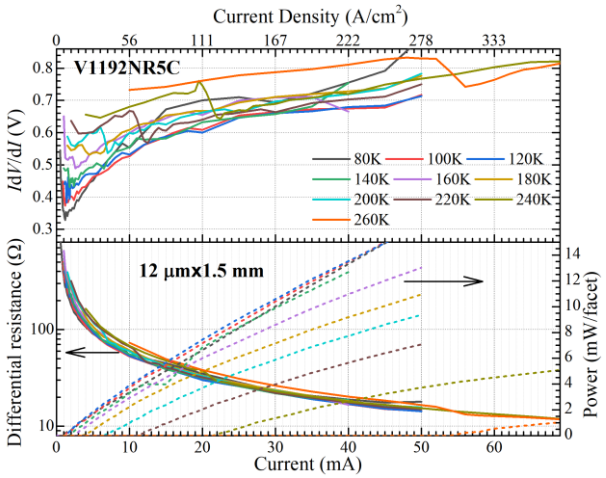

Fig. 17. Differential resistance (bottom), output power (bottom right axis) and IdV/dI (top) for a NR device from V1192 in cw operation at various heat-sink temperatures.

Obvious drops in differential resistance and IdV/dI were observed at the threshold in these InAs-based type-II ICLs in cw operation. Similarly, these drops became somewhat less pronounced at a temperature close to the maximum cw operating temperature. At low temperatures, their threshold current densities were very low. Also, compared to the type-I ICLs in the preceding section, the narrower bandgaps in these devices for the longer lasing wavelengths had a significantly lower differential resistance in individual stages, especially for devices made from V1192 and V1215. The two factors added accuracy limitations to extract their differential resistances at low temperatures with our current experimental set-up. This can be seen from Figs. 16 and 17 where the drops in differential resistance and IdV/dI could not be clearly identified within a small current range at low temperatures. Hence there were relatively large uncertainties and possible errors in the extracted values of ΔR_{th} and $\Delta R_{th}A$ at low temperatures, which are nevertheless kept to give a complete overall picture. With increased numbers of cascade stages, the values of ΔR_{th} and the corresponding $\Delta R_{th}A$ in these ICLs are still comparable to values observed in devices from type-I ICLs, which are shown as a function of temperature in Fig. 18. However, their pinning factor P_f is in the range of 0.1 to 0.6 as shown in Fig. 19, which is somewhat lower than those in type-I ICLs. This may be correlated to the narrower bandgaps and somewhat higher n-type doping (2.6×10^{18} to 3.9×10^{18} cm^{-3}). From the very good linear relationship at relatively low temperatures between the measured output powers of these ICLs (especially BA devices) and the injection current as shown in Figs. 14-17, their slope efficiencies were nearly unchanged with current. This hinted that the carrier concentration (and the quasi-Fermi level) was pinned in these ICLs at the threshold over a wide range of operating temperature. The reduced value of P_f in these ICLs might be again associated with a high n-type doping concentration (in the electron injectors based on the carrier rebalance argument [29]). Such a high doping may have more significant influence in the carrier distribution and transport to these narrow bandgap ICL structures.

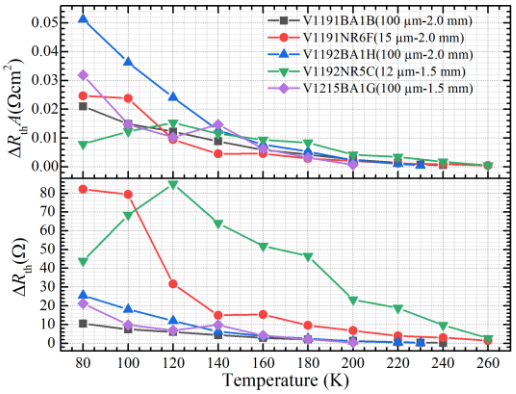

Fig. 18. ΔR_{th} and $\Delta R_{th}A$ as a function of temperature for devices from recent InAs-based type-II ICL wafers.

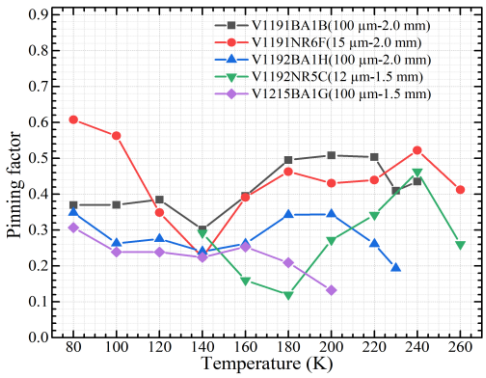

Fig. 19. Pinning factor P_f as a function of temperature for devices from recent InAs-based type-II ICL wafers.

E. Recent Type-II ICLs on a GaSb substrate

Wafer Adv01 is an advanced type-II ICL structure based on the carrier rebalance design [29] with seven (7) cascade stages sandwiched between GaSb SCLs and InAs/AlSb SL cladding layers and grown on a GaSb substrates. BA and NR devices were made from this wafer. These GaSb-based type-II ICLs lased in pulsed mode at temperatures above 400 K and in cw up to 356 K, covering a wavelength range from 2.92 (at 80 K) to 3.57 μm. The relative intensity noise and linewidth broadening factor for these ICLs at room temperature have been recently studied and reported [30-31]. The threshold current density in these ICLs is very low. For example, an ICL had a threshold current density of 143 A/cm^2 in pulsed operation at 300K, which is comparable to the best reported value of ICLs with similar number of cascade stages [2]. As shown in Figs.20-21, output powers of these ICLs at relative low temperatures increased linearly with the injection current and thus their slope efficiencies were nearly unchanged with the current. This implied that the carrier concentration (and the quasi-Fermi level) should be pinned in these ICLs at low temperatures. But, from the obtained I-V curves (shown in Figs. 20-21), the extracted differential resistance did not exhibit an observable drop at the threshold even at low temperatures as illustrated in the top panel of Fig. 21. The lack of drop in differential resistance in these ICLs at threshold may be due to the limited precision and stability of instruments used in experiment combined with the effect of high n-type doping in electron injectors that was mentioned previously for type-I ICLs and recent InAs-based type-II ICLs. This is an observation that is not understood at this moment.

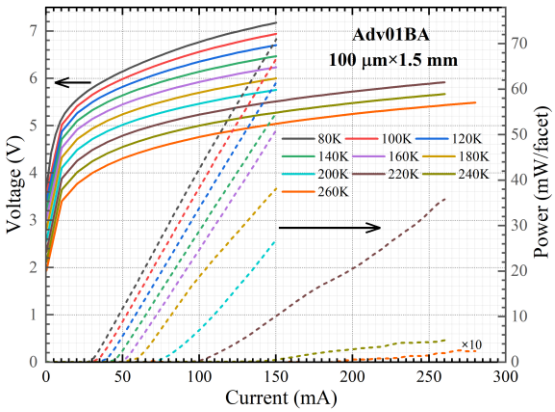

Fig. 20. Current-voltage-light cw characteristics for a BA device from a recent advanced GaSb-based type-II ICL wafer.

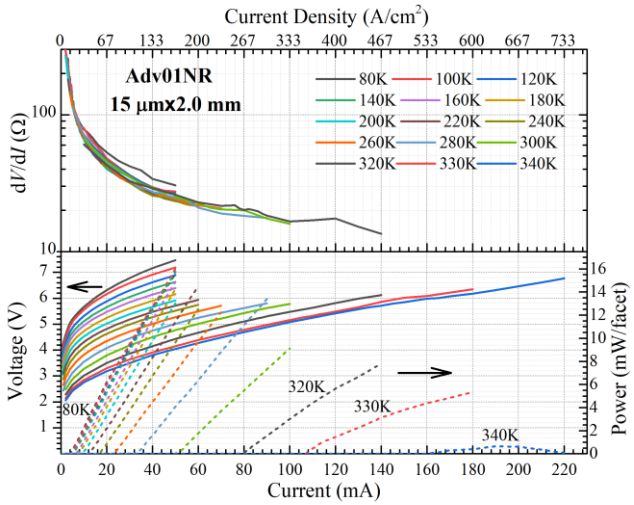

Fig. 21. Current-voltage-light cw characteristics (bottom) and differential resistance (top) for a NR device from a recent advanced GaSb-based type-II ICL wafer.

IV. Summery and Concluding Remarks

Quasi-Fermi level pinning in various ICLs based on type-I or type-II QW active regions is investigated through an extraction of their electrical derivative characteristics. These ICLs grown on either GaSb or InAs substrates comprise different numbers of cascade stages and cover a mid-IR wavelength range from 3 to 6 μm. By extracting an abrupt drop of differential resistance that is proportional to the number of cascade stages, it is revealed that the quasi-Fermi level is pinned at the threshold for many ICLs over a wide range of operating temperature. The quasi-Fermi level pinning does not depend on the choice of QW active regions, consistent with laser principle. Although it is challenging due to much smaller differential resistance in mid-IR lasers with narrower bandgaps compared to that in near-IR lasers, a clear drop of differential resistance at threshold was demonstrated in ICLs at room temperature for the first time, providing an essential evidence of the quasi-Fermi level pinning at threshold for laser operation. This is partially attributed to the series connection of multiple cascade stages, which enhanced the drop of differential resistance at threshold. The quasi-Fermi level pinning becomes weak or disappeared with a soft drop or the lack of an observable drop of differential resistance when the heat-sink temperature was close to the maximum cw operating temperature. How this happened is not understood yet, which might be related to nonuniform temperature distribution in the active regions of a device with substantial heating accumulation or carrier heating as discussed for conventional non-cascade diode lasers in Ref. 23. Differing from the conventional diode lasers, individual QW active regions in an ICL are separated by electron and hole injectors and are connected in series. Hence, individual QW active regions in an ICL can have different temperatures and resistances when there is substantial heat accumulation with large current injection or poor thermal dissipation. Consequently, how individual cascade stages are pinned at the threshold is an open question that needs to be addressed in the future. Methods that can accurately extract differential resistance in pulsed modes with minimized heating effect are needed, which will be helpful to answer this question.

A pinning factor P_f is introduced to fairly evaluate how well the quasi-Fermi level is pinned at the threshold in ICLs with different numbers of cascade stages. It is found experimentally that P_f is higher in ICLs with high defect densities and a relatively low *n*-type doping in electron injectors. In ICLs with relatively high *n*-type doping in electron injectors, P_f is reduced or even disappeared (*i.e.* the quasi-Fermi level pinning is not observable). The correlation between the quasi-Fermi level pinning and the doping in electron injectors, as well as related carrier transport, is not well understood at this stage, but should be interesting topics to be investigated in the future. This may require a detailed study of every involved states in the cascade stages, for example using a rate equation approach coupled with the photon field, since the quasi-Fermi level pinning is a consequence of the optical gain pinning at threshold. A study of QCLs using the rate equation has shown that the drop of differential resistance at threshold could be enhanced or reduced (or even eliminated) depending on the design [32]. Experimentally observed drops of the differential resistance at threshold in QCLs were reported [32-33]. As the quasi-Fermi level pinning has an important impact on device performance characteristics such as output power and wall-plug efficiency, extensive efforts are required to deepen our understanding on this matter, which should shed light on further development of ICLs.

References

1. R. Q. Yang, "Infrared laser based on intersubband transitions in quantum wells," *Superlattices and Microstructures,* vol. 17, no. 1, pp. 77-83, 1995/01/01/ 1995, doi: https://doi.org/10.1006/spmi.1995.1017.
2. I. Vurgaftman, R. Weih, M. Kamp, J R Meyer, C. L. Canedy, C. S. Kim, M. Kim, W. W. Bewley, C. D. Merritt, J. Abell and S. Höfling, "Interband cascade lasers", J. Phys. D: Appl. Phys. **48** 123001 (2015).
3. R. Q. Yang, L. Li, W. Huang, S.M.S. Rassel, J. A. Gupta, A. Bezinger, X. Wu, S.G. Razavipour**,** G. C. Aers, "InAs-based Interband Cascade Lasers", IEEE J. Selected Topics Quantum Electronics, **25**, (6), 1200108 (2019).
4. R. Q. Yang, C. J. Hill, K. Mansour, Y. Qiu, A. Soibel, R. Muller and P. Echternach, "Distributed feedback mid-infrared interband cascade lasers at thermoelectric cooler temperatures", IEEE J. Selected Topics of Quantum Electronics, **13**, 1074 (2007).
5. I. Vurgaftman, W. W. Bewley, C. D. Merritt, C. L. Canedy, M. V. Warren, C. S. Kim and J. R. Meyer, "Sensitive Chemical Detection with Distributed Feedback Interband Cascade Lasers", Encyclopedia of Analytical Chemistry (2016).
6. J. Koeth, R. Weih, J. Scheuermanna, M. Fischera, A. Schadeb, M. Kamp, S. Höfling, "Mid infrared DFB interband cascade lasers", Proc. SPIE, **10403**, Art. No. 1040308 (2017)

7. L. E. Christensen, K. Mansour, and R. Q. Yang, "Thermoelectrically cooled interband cascade laser for field measurements", Optical Engineering, **49**, 111119 (2010).
8. C. R. Webster, P. R. Mahaffy, S. K. Atreya, G. J. Flesch, M. A. Mischna, P.-Y. Meslin, K. A. Farley, P. G. Conrad, L. E. Christensen, A. A. Pavlov, the MSL Science Team, "Mars methane detection and variability at Gale crater", Science **347**, 415 (2015).
9. K. Tanaka, K. Akishima, M. Sekita, K, Tonokura, M. Konno, "Measurement of ethylene in combustion exhaust using a 3.3-μm distributed feedback interband cascade laser with wavelength modulation spectroscopy", Appl. Phys. B **123**, 129 (2017).
10. B. Fang, N. Yang, W. Zhao, C. Wang, W. Zhang, W. Song, D. S. Venables, and W. Chen, "Improved spherical mirror multipass-cell-based interband cascade laser spectrometer for detecting ambient formaldehyde at parts per trillion by volume levels", Applied Optics, Vol. 58, No. 32, 8734 (2019).
11. D. I. Pineda, J. L. Urban, and R. M. Spearrin, "Interband cascade laser absorption of hydrogen chloride for high-temperature thermochemical analysis of fire-resistant polymer reactivity", Applied Optics, **59**, 2141 (2020).
12. R. Q. Yang, "Interband Cascade (IC) Lasers", Chap. 12, in *Semiconductor lasers: Fundamentals and applications*, edited by Baranov and E. Tournie (Woodhead Publishing, 2013).
13. B. A. Ikyo, I. P. Marko, A. R. Adams, S. J. Sweeney, C. L. Canedy, I. Vurgaftman, C. S. Kim, M. Kim, W. W. Bewley, and J. R. Meyer, "Temperature dependence of 4.1 μm midinfrared type II "W" interband cascade lasers temperature dependence of 4.1 μm midinfrared type II "W" interband cascade lasers", Appl. Phys. Lett. **99**, 021102 (2011).
14. C. D. Merritt, W. W. Bewley, C. S. Kim, C. L. Canedy, I. Vurgaftman, J. R. Meyer, and M. Kim, "Gain and loss as a function of current density and temperature in interband cascade lasers", Applied Optics, Vol. 54, F1-F7 (2015).
15. P. M. Smowton and P. Blood, "Fermi level pinning and differential efficiency in GaInP quantum well laser diodes", Appl. Phys. Lett. **70** (9), pp. 1073-1075, 1997.
16. W. Huang, S. M. S. Rassel, L. LI, J. A. Massengale, R. Q. Yang, T. D. Mishima and M. B. Santos, "A unified figure of merit for interband and intersubband cascade devices," Infrared Phys. Technol. **96**, 298 (2019).
17. R. Q. Yang and S. S. Pei, "Novel type-II quantum cascade lasers," *Journal of Applied Physics,* vol. 79, no. 11, pp. 8197-8203, 1996, doi: 10.1063/1.362554.
18. P. Barnes and T. Paoli, "Derivative measurements of the current-voltage characteristics of double-heterostructure injection lasers," *IEEE Journal of Quantum Electronics,* vol. 12, no. 10, pp. 633-639, 1976, doi: 10.1109/JQE.1976.1069050.
19. R. Q. Yang, C. Hill, and B. Yang, "High-temperature and low-threshold midinfrared interband cascade lasers," *Appl. Phys. Lett.,* vol. 87, pp. 151109-151109, 10/04 2005, doi: 10.1063/1.2103387.
20. L. Esaki, L. L. Chang, and E. E. Mendez, "Polytype superlattices and multi-heterojunctions", Jpn. J. Appl. Phys., **20**, L529 (1981).
21. J. R. Meyer, C. A. Hoffman, F. J. Bartoli, L. R. Ram-Mohan, "Type-II quantum-well lasers for the mid-wavelength infrared", Appl. Phys. Lett., **67**, 757 (1995).
22. M. S. Vitiello, G. Scamarcio, V. Spagnolo, W. W. Bewley, M. Kim, C.-S. Kim, I. Vurgaftman, J. R. Meyer, and A. Lops, "Microprobe photoluminescence assessment of the wall-plug efficiency in interband cascade lasers", Appl. Phys. Lett. **104**, 046101, 2008
23. M. Y. Vinnichenko, L. E. Vorobjev, D. A. Firsov, M. O. Mashko, R. M. Balagula, G. Belenky, L. Shterengas, and G. Kipshidze, "Dependence of the carrier concentration on the current in mid-infrared injection lasers with quantum wells," Semiconductors **47**, 1513–1516 (2013).
24. J. D. Bruno, J. L. Bradshaw, R. Q. Yang, J. T. Pham, and D. E.Wortman, "Low-threshold interband cascade lasers with power efficiency exceeding 9%," *Appl. Phys. Lett.*, vol. 76, pp. 3167–3169, May 2000.
25. R. Q. Yang, J. L. Bradshaw, J. D. Bruno, J. T. Pham, and D. E.Wortman, "Power, efficiency, and thermal characteristics of type-II interband cascade lasers," *IEEE J. Quantum Electron.*, vol. 37, pp. 282–289, Feb. 2001.
26. K. Mansour, C. J. Hill, Y. Qiu, R. Q. Yang, "Dual-Wavelength Interband Cascade Lasers in Mid-Infrared Spectral Region", Proc. The Conference on Lasers and Electro-Optics (CLEO) and the Quantum Electronics and Laser Science Conference (QELS), paper CTuZ4, 2008.
27. Z. Tian, Y. Jiang, L. Li, R. T. Hinkey, Z. Yin, R. Q. Yang, T. D. Mishima, M. B. Santos, and M. B. Johnson, "InAs-Based Mid-Infrared Interband Cascade Lasers Near 5.3 μm," *IEEE Journal of Quantum Electronics,* vol. 48, no. 7, pp. 915-921, 2012, doi: 10.1109/JQE.2012.2195477.
28. Y. Jiang, L. Li, R. Q. Yang, J. A. Gupta, G. C. Aers, E. Dupont, J. Baribeau, X. Wu, and M. B. Johnson, "Type-I interband cascade lasers near 3.2 μm," *Appl. Phys. Lett.*, vol. 106, 2015, Art. no. 041117.
29. I. Vurgaftman, W. W. Bewley, C. L. Canedy, C. S. Kim, M. Kim, C. D. Merritt, J. Abell, J. R. Lindle, and J. R. Meyer, "Rebalancing of internally generated carriers for mid-infrared interband cascade lasers with very low power consumption," Nat. Commun. **2**, 585 (2011).
30. Y. Deng, B.-B. Zhao, Y.-T. Gu, and C. Wang, "Relative intensity noise of a continuous-wave interband cascade laser at room temperature," *Opt. Lett.,* vol. 44, no. 6, pp. 1375-1378, 2019, doi: 10.1364/OL.44.001375.
31. Y. Deng, B.-B. Zhao, and C. Wang, "Linewidth broadening factor of an interband cascade laser," Appl. Phys. Lett. vol. 115, no. 18, Art. No. 181101, 2019, doi: 10.1063/1.5123005.
32. C. Sirtori, F. Capasso, J. Faist, A. L. Hutchinson, D. L. Sivco and A. Y. Cho, "Resonant tunneling in quantum cascade lasers", IEEE Journal of Quantum Electronics, vol. 34: no. 9, pp. 1722-1729, 1998.
33. M. Beck, D. Hofstetter, T. Aellen, J. Faist, U. Oesterle, M. Ilegems, E. Gini and H. Melchior, "Continuous wave operation of a mid-infrared semiconductor laser at room temperature", Science, vol. 295: no. 5553, pp. 301-305, 2002.

.

Yuzhe Lin received the B.S. degree in microelectronics from Sichuan University, Chengdu, China, in 2014. He is a graduate student with Institute of Semiconductors, Chinese Academy of Sciences, currently as a visiting scholar with the School of Electrical and Computer Engineering, University of Oklahoma. His research interests include the design, fabrication and test of edge-emitting laser diodes.

Lu Li received the Ph.D. degree in material sciences from the Institute of Semiconductors, Chinese Academy of Sciences, Beijing, China, in 2008. He worked at the University of Oklahoma, Norman, USA as a postdoctoral researcher from October 2010 to November 2018, with research interests on the materials and devices related to the interband cascade lasers and photodetectors. He is currently working on the III-V near-infrared lasers at Lumentum Operation LLC, San Jose, CA, USA. He has authored or co-authored more than 100 scientific publications.

Wenxiang Huang (GSM'18), received the B.S. and M.S. degrees in physics from Shandong University, Jinan, China, in 2012 and 2015, respectively. He is currently pursuing the Ph.D. degree in engineering physics at the University of Oklahoma, Norman. His research interest includes modeling and characterization of infrared optoelectronic devices such as photodetectors, thermophotovoltaics and lasers based on interband cascade structures.

Rui Q. Yang received his Ph.D. degree in physics in 1987 and is a professor at University of Oklahoma. Prior to joining University of Oklahoma in 2007, he was a Principal Member of Engineering Staff and a Task Manager at the Jet Propulsion Laboratory, California Institute of Technology, Pasadena, California, where he led the development of advanced interband cascade lasers for applications in Earth sciences and planetary explorations. He is a Fellow of OSA and the recipient of 2018 IEEE Photonics Society Aron Kressel Award. He has authored/co-authored more than 140 articles in peer-reviewed journals.

James A. Gupta received his Ph.D. in Physics from Simon Fraser University in British Columbia, Canada. He has been at the National Research Council of Canada since 1999. He is the primary molecular beam epitaxy scientist for all arsenide and antimonide materials and is the scientific lead for mid-infrared laser development. He has co-authored more than 100 articles in peer-reviewed journals.

Wanhua Zheng (M'06) received the M.Sc. degree from the Institute of Physics, Chinese Academy of Sciences (CAS), Beijing, and the Ph.D. degree from Baptist University, Hong Kong, in 1991 and 1998, respectively. She is currently a Professor in the Institute of Semiconductors, CAS, where she joined in 1991. She was previously with Optoelectronics Laboratories, University of New South Wales, Sydney, Australia, from 2001 to 2003, where she pioneered the first wideband laser mirrors based on 1-D porous silicon photonic crystals. Her research interests include modeling and processing of photonic band-gap materials and devices, and nanophotonic integrated circuits.